JOINT EUROPEAN TORUS

JET-P(89)48

A. Boileau, L. Horton, W. Mandl, H.P. Summers,
M. von Hellermann and H. Weisen

Charge Exchange Spectroscopy Measurements of Ion Temperature and Toroidal Rotation in JET

Charge Exchange Spectroscopy Measurements of Ion Temperature and Toroidal Rotation in JET

A. Boileau[2], L. Horton[3], W. Mandl[4], H.P. Summers,
M. von Hellermann and H. Weisen[1]

JET Joint Undertaking, Culham Science Centre, OX14 3DB, Abingdon, UK

[1]*CRPP-EPFL, 21, av. des Bains, CH-1007 Lausanne, Switzerland*
[2]*IREQ, 1804 Montée Ste Julie, Varennes, PQ JOL-2PO Canada*
[3]*ORNL, Oak Ridge, Tennessee 37831, U.S.A.*
[4]*IPP, 8046 Garching, F.R.G.*

Preprint of a paper to be submitted for publication in
Nuclear Fusion

ABSTRACT.

The JET tokamak relies on an active charge exchange spectroscopy diagnostic for measurements of ion temperature, toroidal rotation velocity and impurity density profiles. It uses the neutral heating beams as diagnostic beams and provides measurements at 8 to 12 radial positions simultaneously with a time resolution of about 100ms. A description of the instrument is given, together with a presentation on the analysis of the experimental data and an account on recent results. Profiles of ion temperature and rotation frequency based on the carbon CVI n = B to n = 7 transition at 5290.5Å are presented for plasmas in the hot ion mode, for magnetic limiter plasmas, and for discharges where a locked MHD mode brings the plasma to rest despite continued neutral beam injection. H to L-mode transitions are found to cause a collapse of the edge ion toroidal rotation frequency within less than a sampling time time resolution is also sufficient to reveal ion heat sawtooth crashes.

1. INTRODUCTION

Charge exchange reactions between neutral particles and plasma ions provide a unique method to measure the distribution functions of the ion species present in a hot plasma. The application of active charge exchange spectroscopy (CXS) to the measurement of impurity ion temperatures and toroidal rotation velocities in tokamaks is well established [1-8]. Thermal and bulk ion velocities are obtained from the Doppler effect on emission lines from hydrogen-like ions resulting from charge exchange reactions of fully stripped bulk plasma ions with injected fast hydrogen or deuterium neutrals. These hydrogen-like ions are created in an excited state and promptly cascade to lower quantum states.

CXS measurements based on visible transitions benefit from the availability of high resolution spectrometers and straightforward calibration techniques for absolute impurity density measurements. Since quartz fibres can be used to transmit the collected light, the CXS diagnostic at JET makes extensive use of the visible wavelength range in view of the active tritium phase, when all instrumentation will be required to be be located outside the torus hall beyond the biological shield. The restriction to the visible wavelength range is not a severe constraint since all the light ion species which constitute the bulk of most tokamak plasmas have suitable charge exchange transitions in the visible.

In JET the neutral heating beams are employed as diagnostic beams and ion temperature and rotation velocity profiles from CXS are routinely available for JET discharges with neutral beam injection [9-12]. Further applications at JET not included in this paper are routine measurements of absolute impurity densities [13-15] and the proposed measurement of the low energy part of slowing down Alpha particle distribution during the tritium phase [16]. Recently the dicovery of motional Stark features in the Balmer spectrum of the beam deuterons has extended the capabilities of this diagnostic to include local magnetic field measurements [17].

In the following section we present a detailed description of the experimental configuration of the JET CXS profile diagnostic. In section 3 the data analysis procedure is presented. The influence of background features and parasitic effects such as emission from circulating ions produced by charge exchange reactions are assessed. A selection of results from ion

temperature and rotation measurements are presented and discussed in sections 4 and 5.

2. EXPERIMENTAL ARRANGEMENT

The JET active charge exchange diagnostic includes a set of 15 horizontal viewing lines for profile measurements and one vertical viewing line for single point measurements at the plasma centre (fig.1). The quartz viewing optics of the multi-chord system at point (A) in fig.1a form an image of the beam region onto the ends of 15 PCS1000 quartz fibres, defining 15 nearly horizontal viewing lines intersecting the neutral heating beams from the neutral injector at octant 8 at major radii between 2.7 and 4.0 m (fig.2). The fibre ends are arranged in a stack with a separation of 1.5 mm between adjacent fibres. To produce this arrangement the stacked fibres were cemented into a slotted end-plate and polished together. The plate was then mounted in the focal plane of the viewing optics as shown in fig.2. The beam region is viewed indirectly via a Nickel mirror which can be folded back to protect itself, and the quartz vacuum window behind it, from being coated during discharge cleaning or evaporative deposition inside the vessel of a beryllium gettering layer.

The collected light is relayed to the diagnostics hall by 90 m of radiation resistant optical fibres onto a SPEX 1269 spectrometer (f=1.27m) equipped with a vidicon array (EG&G 1254, 500×512 pixels, spaced 25 μ) allowing simultaneous recording of multiple (initially 8, now 12) spectra. A subset of 8 (respectively 12) of the 15 fibres is coupled to the spectrometer. The fibre ends are arranged in a vertical stack similar to the one described above and are imaged onto the entrance slit of the spectrometer using commercial photo lenses.The vidicon detector mounted at the spectrometer exit side was divided into 8 (respectively 12) horizontal tracks by grouping the individual pixels into 'superpixels' of a size of 1×64 (respectively 1×30 to 1×40) pixels. The absolute overall sensitivity of the system is recalibrated at each major maintenance period of the JET device using an irradiance standard placed in front of the viewing mirror.

A number of drawbacks related to the use of the vidicon required special attention. They include pincussion distortion in the readout electron optics, a smaller than expected usable dynamic range due to detector non-linearity and charge diffusion (above about 3000 counts per superpixel as compared to about 10 counts of background noise level), and incomplete charge readout. The

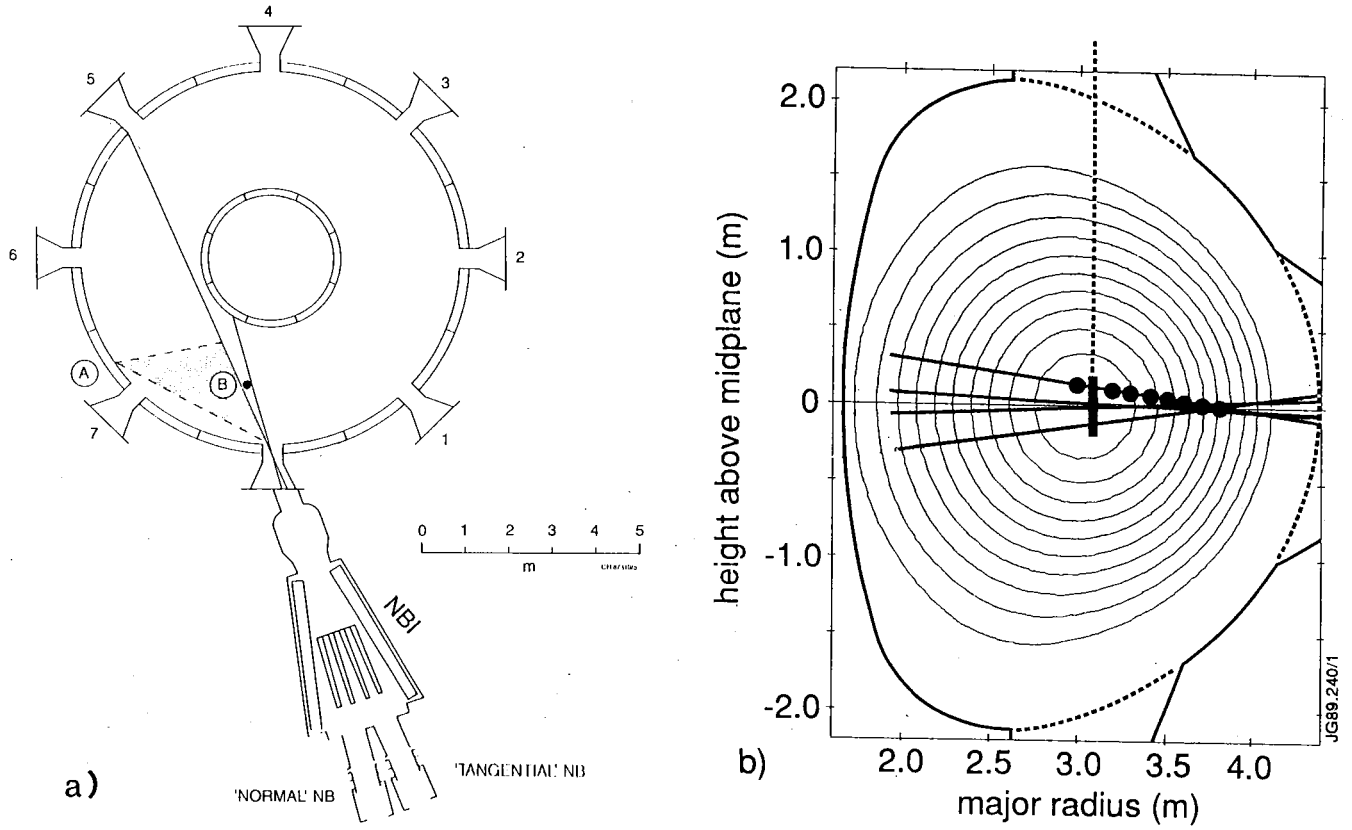

Fig.1 Arrangement of CXS viewing lines.

a) (A) Location of collection optics of multichord system, (B) Tangential and normal beam lines, with vertical viewing line in between. b) Viewing volumes along beam path.

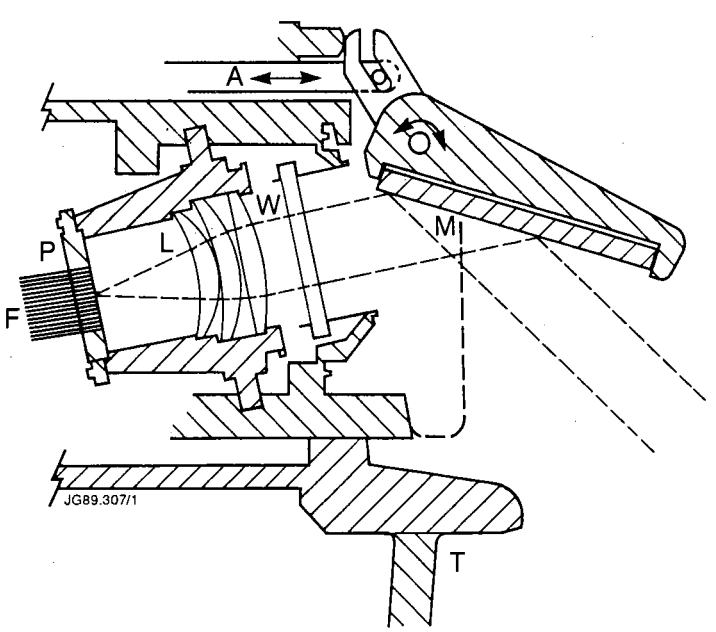

Fig.2 Outline of multichord viewing optics .

F) Optical fibres, P) Fibre mounting plate, L) imaging lens arrangement, W) vacuum window, M) Nickel mirror A) mirror actuator.

latter affects mostly the weaker signals from the plasma core, leading to a temporal smearing-out over consecutively recorded time frames and thus loss of time resolution. The pincushion distortion of the electron optics causes the magnification to increase towards the array boundaries, effectively increasing the dispersion expressed in Å per pixel. Relative differences in dispersion between different areas of the vidicon are up to 15% for the central 300×512 pixels which were used for the measurements. This effect was corrected for by a measurement of the local dispersion at 11 positions on each track using a pair of mercury lines stepped accross the array. Hence the effective dispersion is calibrated to an accuracy better than 1%. Crosstalk between tracks as a result of pincushion distortion was found to be negligible.

The spectrometer grating of 600 lines/mm used for most of the profile measurements provided a dispersion at the vidicon of 0.325 Å per pixel at a centre wavelength of 5290.5 Å. The slit width was kept to 100 or 200μ for instrument function widths of 1.2 or 2.4 Å, as compared to a Doppler broadening of 12 Å for 10 keV carbon ions emitting at 5290.5 Å. The spectra are deconvolved with the instrument function represented by a sum of Gaussians to allow temperature measurements down to about 50 eV.

The single chord system with a vertical viewing line at R=3.1 m uses a beamsplitter and two spectrometers equipped with linear reticon arrays (EG&G 1420), dedicated to central carbon and oxygen CXS measurements respectively. A detailed description of this system can be found in an earlier publication [13]. Sampling times are typically 100 ms for the multichord system, but have been as short as 12 ms for the single point system.

The two JET neutral beam injectors are symetrically located in the torus octants 8 and 4. The former is used for active CXS and is shown in fig.1a. The injectors consist of 8 subunits with a power of 1.2 MW each, and are divided into a 'tangential' bank and a 'normal' bank, each with 4 beams firing at angles of $\pm 3^{\circ}$ and $\pm 9^{\circ}$ with respect to the midplane (fig.1b). The acceleration voltage is 80 keV for Deuterium. Full, half and third energy components are present in the proportions of 0.76:0.17:0.07 [18]. The beam intensity profiles were found to be well discribed by Gaussians with 1/e widths of the order of 20 cm. When only one of the neutral beam banks ('normal' or 'tangential') is fired, the localisation is better than ± 3 cm in major radius. The accuracy of the alignement is regularly reassessed by measuring the Doppler shift of excited Balmer-α beam components, which provides the angle between the viewing lines and the beam direction. In most cases of high power neutral heating

beams from both banks contribute to the charge exchange signal. The positions indicated then are a weighted average over the contributions from the different beams. The intersections with the tangential and normal beam lines are always less than 10 cm apart in major radius.

3. DATA ANALYSIS

An analysis of the dominant CX spectra and their specific features, which are observed in neutral beam heated JET plasmas, was described in earlier papers [13,19,20]. They include the main visible transitions of the dominant light impurities such as oxygen (OVIII n=9 to n=8 and n=10 to n=9), carbon (CVI 8-7, and 10-8), helium (HeII, 4-3), and those of the bulk plasma deuterons (DI, 3-2 and 4-2). Following the recent introduction of beryllium into the JET device, the CX line of BeIV (6-5) at 4659 Å was succesfully analysed in the presence of the CX spectrum of the HeII transition at 4685 Å. Carbon being the dominant impurity in JET plasmas, most of our measurements are based on the 8-7 transition of Carbon VI at 5290.5 Å.

The doppler broadening and the line center displacement provide the impurity ion temperature and the toroidal rotation velocity. Absolute impurity densities are inferred from the measured line intensities and the local beam intensity obtained from a beam attenuation calculation [14].

Depending on plasma conditions and viewing lines, a 'cold' spectral component from emission at the plasma edge may be present in addition to the CX feature (fig. 3). This 'cold' component at 5290.5 Å is due to electron impact excitation of C VI and O VI present in the edge or to CX reactions of fully stripped carbon ions and O VII from the edge plasma with slow neutrals originating from walls and limiters. When necessary this and possible neighbouring lines are taken into account by a multi-Gaussian fit on the measured spectra. In most cases the cold component at 5290.5 Å can be represented by a Gaussian distribution with a temperature of 0.4 to 1.2 keV and is therefore readily distinguished from the generally much hotter CX emission. The cold component from CVI and OVI at 5290.5 Å in the absence of NBI is used as a wavelength reference for the angular frequency measurements. Since the introduction of beryllium into the JET device, a narrow BeII line at 5270.7 Å with an apparent temperature below 100 eV is used as a reference.

The cold component and the CX component near the edge are usually not different enough in temperature to allow them to be unambigously distinguished

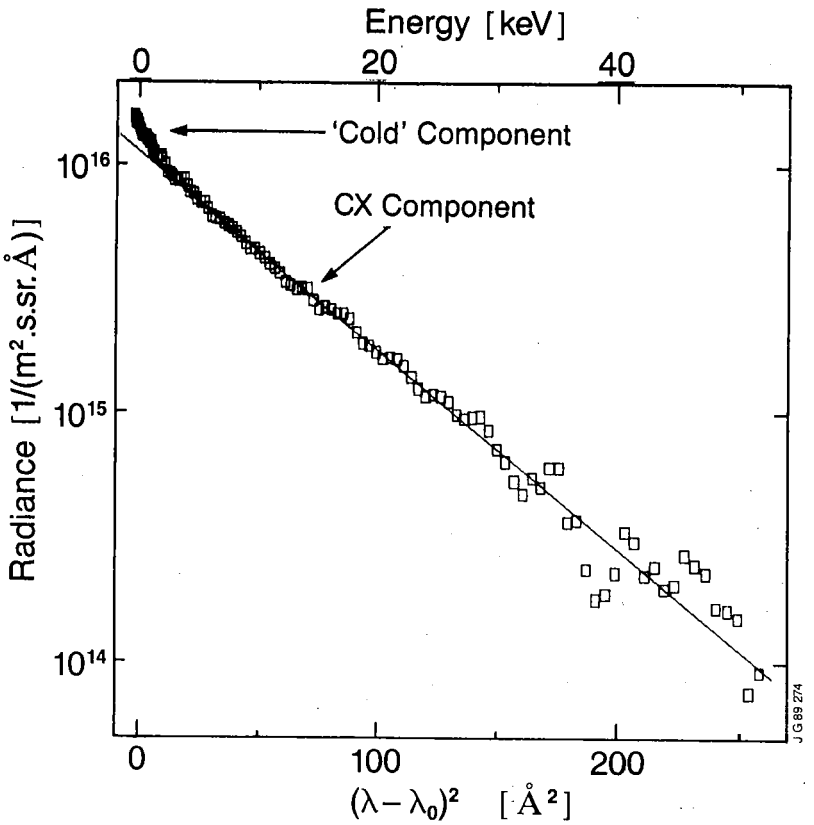

Fig.3 Example of CX spectrum obtained in JET

Vertical viewing line, C^{+5} n = 8 to 7 at 5290.5 Å, $T_i(0)$ = 10.2 keV. To show the maxwellian distribution of the charge exchange component, the measured photon flux is plotted on a logarithmic scale versus the square of the wavelength shift, $(\lambda - \lambda_0)^2$, which is proportional to the kinetic energy parallel to the viewing direction of the emitting ions. Two gaussians were fitted to account for a 'cold' component emitted near the plasma edge. The influence of the cold component is restricted to energies below about 3 keV.

by fitting two Gaussians. Fortunately these channels benefit from the very strong CX emission in this region as a result of the superposition in the outer midplane of all 8 neutral beams and yet small beam attenuation. Since the charge exchange signals in the outermost channels are up to 100 times stronger than the cold component, they require only a single Gaussian to be fitted to the spectra. The charge exchange signals from the central channels of the multichord system are typically 10 to 20 times weaker than the signals from the outermost positions and require the cold component to be taken into account in most conditions.

The differences in photon flux from the charge exchange lines accross the

profile are also reflected in the statistical fitting errors (standard deviation) on the ion temperature deduced from the C^{+5} line at 5290.5 Å, which increase from about 2% near the edge to 5-10% at R ≅ 3.0 m, depending on beam attenuation and carbon density. (In some cases of very high plasma density the innermost channels have to be excluded from the analysis.)

The measurements can be affected by radiation from hydrogen-like ions produced by charge exchange reactions outside the observation volume which subsequently drift along the field lines into the line of sight, and are reexcited by electron impact [4,7]. For typical JET conditions ($n_e \cong 3\times10^{19}$ m^{-3}, $T_i \cong 10$ keV) the ionisation rate of C^{+5} is sufficiently low to allow these ions to drift a few times around the torus before being reionized ($\sigma v = 1.36\times10^{-16}$ m^3s^{-1} for $T_e = 10$ keV). Hence the emission from the C^{+5} 'plumes' produced by the neutral injectors in both octant 4 and octant 8 can interfere with the measurement.

We have investigated this effect for JET pulses when only the beams in octant 4, which are not viewed by the CXS diagnostic, were fired. We found that this emission was comparable in linewidth and linecentre to the usual charge exchange emission, i.e. had apparent temperatures and toroidal rotation velocities characteristic of the bulk (rather than the edge) plasma. This is what is expected since plume emission is is detected from along the entire viewing chord which spans a wide range of plasma parameters. The pulses investigated covered plasma parameters representative of normal operating conditions ($n_e \cong 1$ to 5 $\times10^{19}m^{-3}$, Te(0) ≅ 4 to 8 keV, Ti(0) ≅ 4 to 12 keV). The ratio of photon flux from the plume effect to that from direct charge exchange emission was found to rise from about 2% for the outermost chord intersecting the beams at 3.8 m, to between 10 and 20% for a chord at 3 m. This ratio was typically between 5 and 10% for the vertical viewing line. Since the apparent temperature of this parasitic emission is not very different from the direct charge exchange emission it cannot be isolated by a multi-Gaussian fit and will bias the temperature and angular velocity measurements. The resulting errors are negligible for R≥3.4 m, where charge exchange emission dominates. A systematic bias towards lower temperatures and rotation velocities is to be expected for the innermost channels. From the ratio of CX to plume emission and respective temperatures we estimated that this bias can be as large as 10% at R=3.0 m.

Distortions of the charge exchange spectra from the shape of the original

ion distribution function can arise as a result of the dependence of the charge exchange excitation rates on the velocities of the impurity ions with respect to the beam neutrals [21,22]. The intensity of the red (blue) wing of the CX spectrum may therefore be enhanced with respect to the blue (red) wing depending on the beam energy, the energy dependence of the charge capture cross sections, and the direction of observation. For a thermal ion population the resulting spectrum is still accurately fitted by a Gaussian. However, for the viewing geometry of the JET multichord system, the effect leads to an apparent blue shift of the charge exchange line, which increases with ion temperature. A change in the line width, affecting the ion temperature measurement, is also to be expected.

The theoretical effective cross sections are well established at energies of 40 keV/amu and above, but were sparse and have shown differences at lower energies [23-25]. Recent theoretical calculations [26] have been made available and specific experiments [27] have been initiated to close the gaps in the low energy range and provide the data needed to calculate (and correct for) this effect.

Experimentally this apparent blue shift is clearly observed with deuterium charge exchange spectra, but it appears not to affect our rotation measurements derived from the C^{+6} 8-7 transition beyond the usual uncertainties (about 5000 rad/sec). No clear evidence for the effect was found in discharges where the bulk plasma remained at rest during neutral heating to temperatures of up to 10 keV (such a discharge is presented in section 5).

The energy dependence of the charge exchange cross section causes the derived ion temperatures to become biased towards lower values. The effect increases with ion temperature and is strongest for Deuterium ions because of their higher thermal velocity. Experimentally at fairly low temperatures (3 keV) the (uncorrected) central deuterium temperatures from the multipoint system are found to be about 7% lower than simultaneously measured carbon temperatures using the vertical viewing line. This is consistent with recently published charge transfer cross sections by Fritsch [26]. Simulations of the spectral distortion based on these cross sections suggest that this biasing to lower temperatures is below a few percent for our usual n=8 to n=7 transition of C^{+5}, at a temperature of 20 keV, and as high as 25% for the deuterium Balmer-α transition.

4. RESULTS

The diversity of JET operating and heating scenarios is reflected in the ion temperature profiles observed under various conditions. They range from the 600 eV 'cold' and entirely flat profiles, produced by the injection of a pellet into an ohmic plasma, at the lower end, to highly peaked hot ion mode profiles at the other extreme, where temperatures of up to 27 keV have been achieved. Many of our results have already been presented in relation with specific topics, like heat and impurity transport analysis [28], correlation of toroidal rotation with MHD activity and frequency [29], or general performance assessments of the JET device [30]. We shall therefore present a selection of results which are representative for plasma conditions recently achieved at JET, as well as new observations with a bearing on the transport of ion thermal energy and toroidal momentum.

The highest ion temperatures and rotation velocities are obtained with high power neutral beam heating of a low density ($n_e(0) \leq 10^{19} m^{-3}$) target plasma such that electrons and ions are decoupled. Peak ion temperatures can exceed the electron temperature by more than a factor of three. These discharges are characterised by very peaked ion temperature and toroidal rotation velocity profiles as shown on fig.4 for a case with 20 MW of NBI heating and 3 MW of RF heating. Such conditions have only been obtained transiently since after about 0.6 sec following application of NBI a strong influx of carbon released from hot spots at the carbon tiled walls and carbon limiters degraded the plasma.

The broadest ion temperature profiles are obtained in magnetic limiter discharges. In this configuration an improved confinement regime (H-mode) is obtained [31]. Fig.5 shows ion temperature and rotation profiles during an H-mode and an immediately subsequent phase of low confinement (L-mode). Note that there appears to be a flattened central zone and a clear linear gradient zone for $R > 3.4$ m delimited by the $q=1$ surface as determined from the sawteeth inversion radius. There is close agreement with the electron temperature obtained from the LIDAR Thomson scattering system, alsoshown in fig.5. (It should be noted that the Te and Ti profiles were not obtained at the same time, nor at the same phase of the sawtooth cycle). The angular rotation frequency at the $q=1$ surface coincides with the frequency of $n=1$ MHD oscillations associated with sawtooth activity as measured by external magnetic probes. It thus appears that the magnetic perturbations at the $q=1$ surface are pulled along with the plasma as it is spun up by the beams.

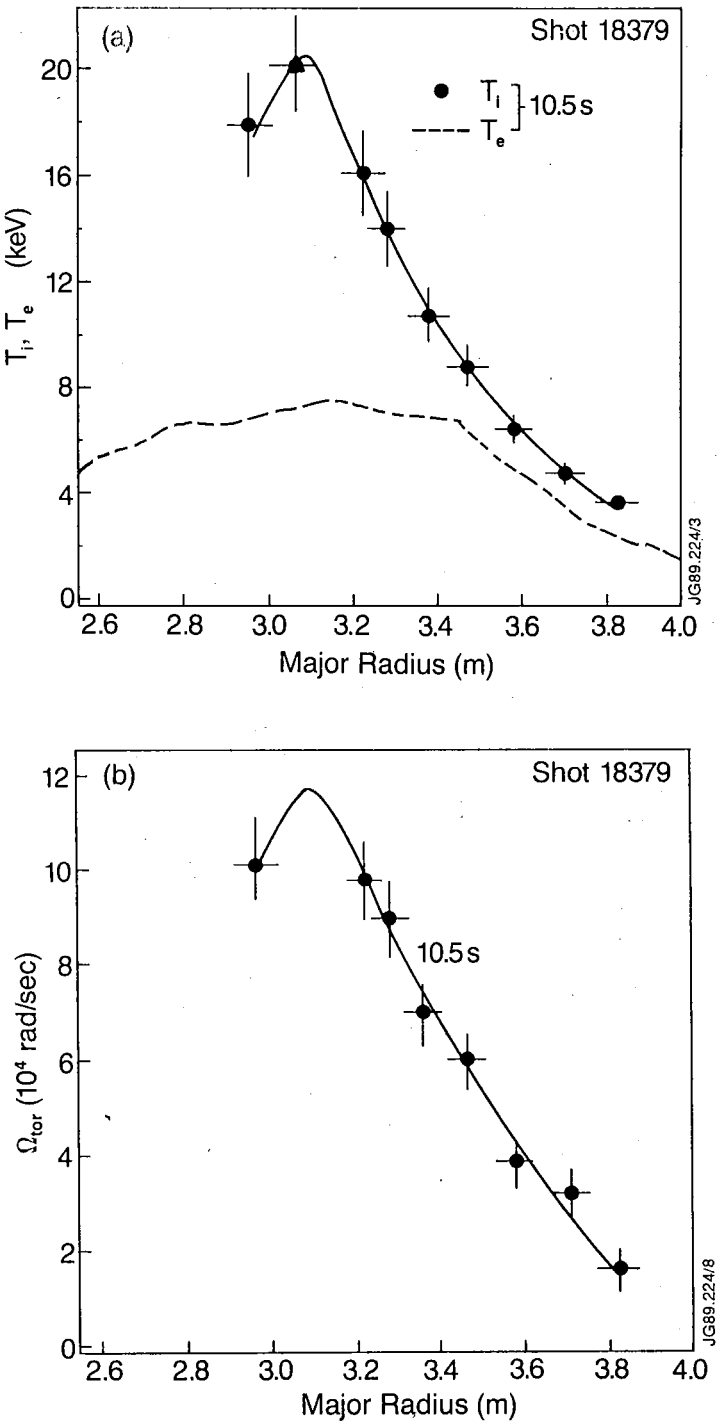

Fig.4 Hot ion mode plasma.

a) Ion and electron temperature profiles. b) Angular velocity profile.

I_p=3 MA, B_T=3 T, $n_e(o)=2\cdot10^{19}$ m^{-3} for t=10.5 s, P_{NBI}=20 MW, P_{RF}=2 MW.

The positions shown are the intersections of the magnetic flux surfaces containing the observation volumes with the plasma midplane. The measurement using the vertical viewing line is shown as a triangle. The electron temperature profile was obtained from the LIDAR Thomson scattering system.

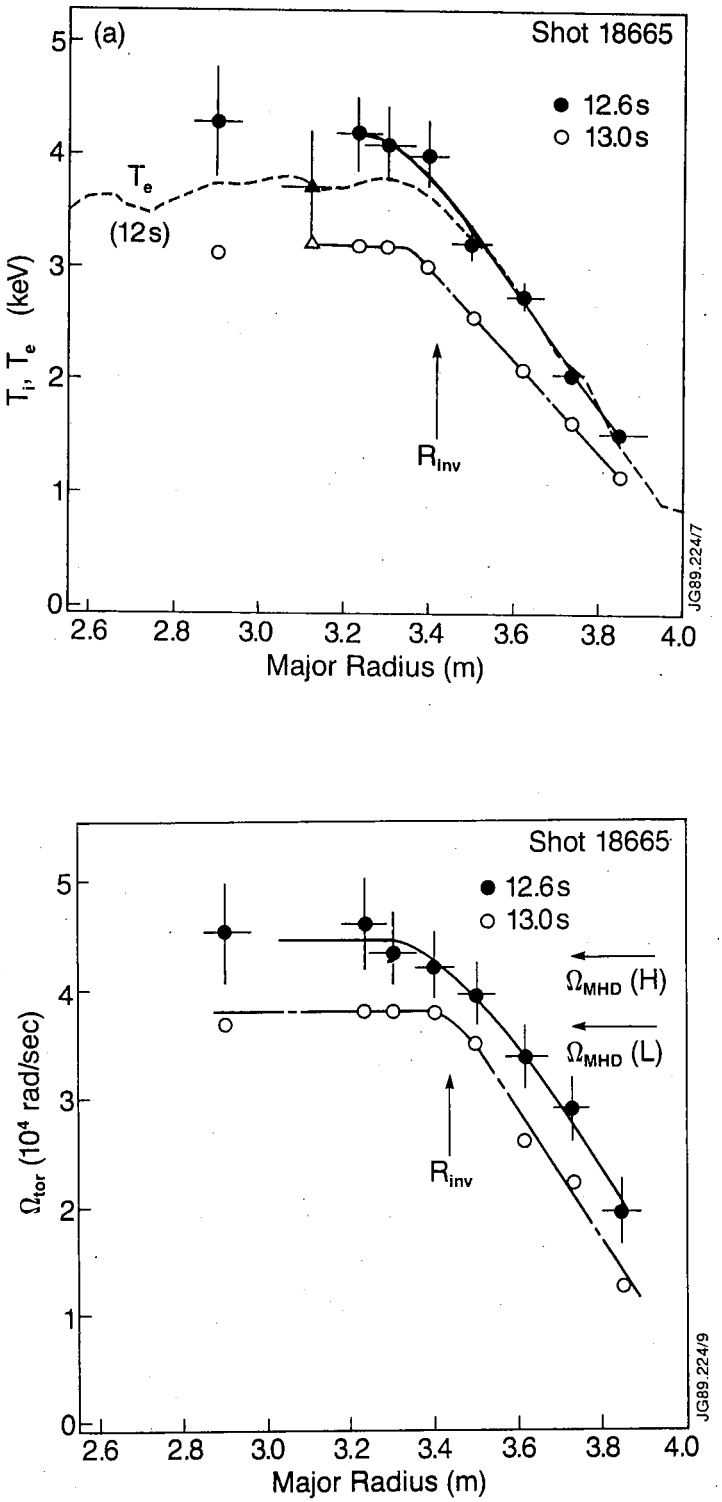

Fig.5 Magnetic limiter plasma in H (12, 12.6 s) and in L mode (13s). a) Ion and electron temperature plasmas. b) Angular velocity profiles. The horizontal arrows in b) indicate the frequency of n=1 sawtooth pre and postcursor oscillations. I_P=3 MA, B_T=2.1 T, $n_e(0)=3.5\cdot10^{19}$ m^{-3}, P_{NBI}=6 MW. The sawteeth inversion radius is denoted by R_{inv}.

The transition from the H-mode back to the L-mode occurs at a time scale that is too short to be resolved by the Vidicon detector. Fig. 6 shows a single point measurement at R=3.82 m (0.20 m inside the separatrix) obtained using one of the linear arrays with a sampling time of 12 ms. This discharge featured two successive quiescent H-mode phases, indicated by phases of low D_α emission in the figure. The overall temporal evolutions of the toroidal velocity and the ion temperature are very similar, in many cases they remain proportional to each other within less than 10%. We observe that at an H to L transition both the ion temperature and, remarkably, the toroidal rotation

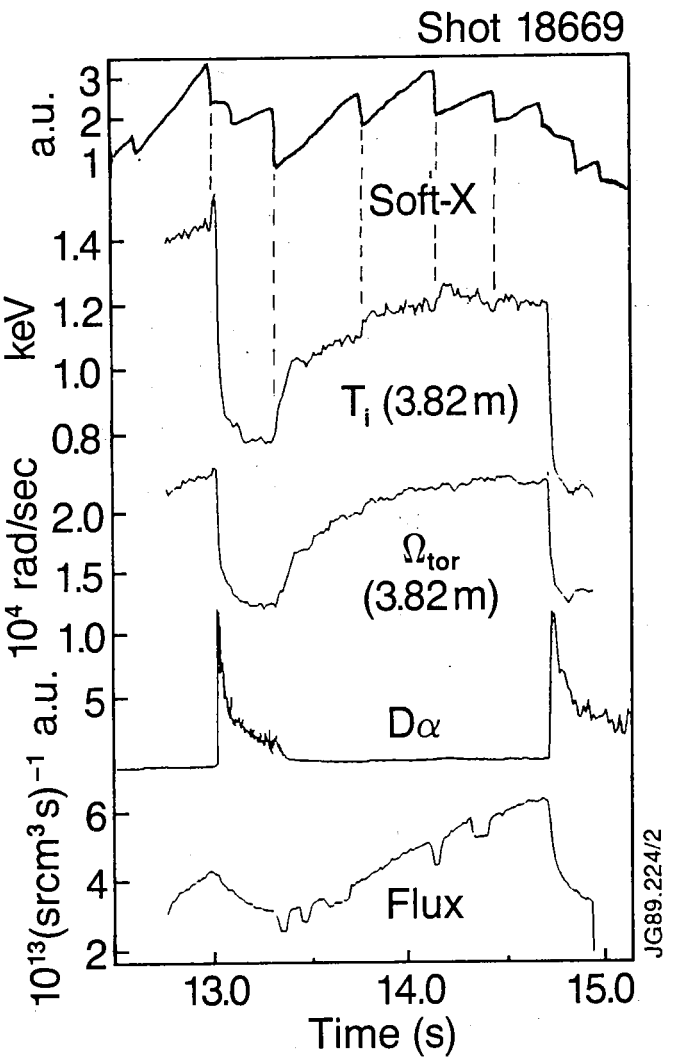

Fig.6 Transition events in a magnetic limiter plasma. CXS measurement at R=3.82 m of T_i and angular velocity Ω_{tor} with 12 ms resolution. B_T=2.1 T, I_P=3 MA, P_{NBI}=10 MW. (The notches in the bottom trace, which shows the photon flux from the CX line, are due to intermittent beam failures). The top trace shows a sawtoothing soft X ray signal. The D_α signal indicates H and L mode phases.

velocity decrease to their L-mode values within less than a sampling time. A similar fast drop of rotation velocity at the H to L transition is observed by passive spectroscopy on the Doublet III tokamak within 1 to 3 cm inside the separatrix [32]. The fast evolution of the ion temperature and rotation is in contrast with the behavior of both the electron and the carbon ion densities, which decay with time scales in the range of 100-200 ms, implying decoupled energy and particle transport at the transition event. The beams are little attenuated at R=3.82 m, thus the the photon flux from the CXS line shown in fig.6 is a measure of the C^{+6} density when the beam power is kept constant. The behavior at the H to L transitions appears to differ from the behavior at isolated edge localised modes (ELMs), where energy losses can be attributed to an outward convection and loss of particles in the outer $\approx$10 cm of the discharge on a time scale of the order of 50 μs [33].

Fig. 7 shows a case of a brief H-mode with ELMs revealed by the spikes of the D_α signal. ELM's depress the ion temperature and rotation velocity. Pulse-like inverted ion temperature sawteeth are visible on both figures 6 and 7. Their rapid decay in the case of the 'ELMY' discharge suggests that the heat released at the sawtooth crash is rapidly lost at the edge, whereas in quiescent H-modes it can contribute to the buildup of an edge pedestal as a consequence of improved edge confinement. Despite the fairly long sampling time of 12 ms these ion heat pulses are very similar both in amplitude and rise time (20 - 30 ms) to electron heat pulses measured using electron cyclotron emission. Sawtooth related events are remarkably absent from our rotation data at R=3.82 m and high sampling rate. Such data have so far only been obtained for magnetic limiter plasmas.

5. DISCUSSION

The similarity of ion temperature and toroidal rotation profiles and time evolution in many cases of NBI heated discharges, together with the identical shapes of the beam energy and toroidal angular momentum deposition profiles, suggests that heat and momentum transport may be governed by related mechanisms and have similar confinement times. A close connection between these two quantities has also been found on the DIII tokamak [8]. Ion temperature gradient driven turbulent transport, with identical ion thermal diffusivity and shear viscosity, has been proposed as an explanation for this relationship [34]. We wish to point out observations showing the

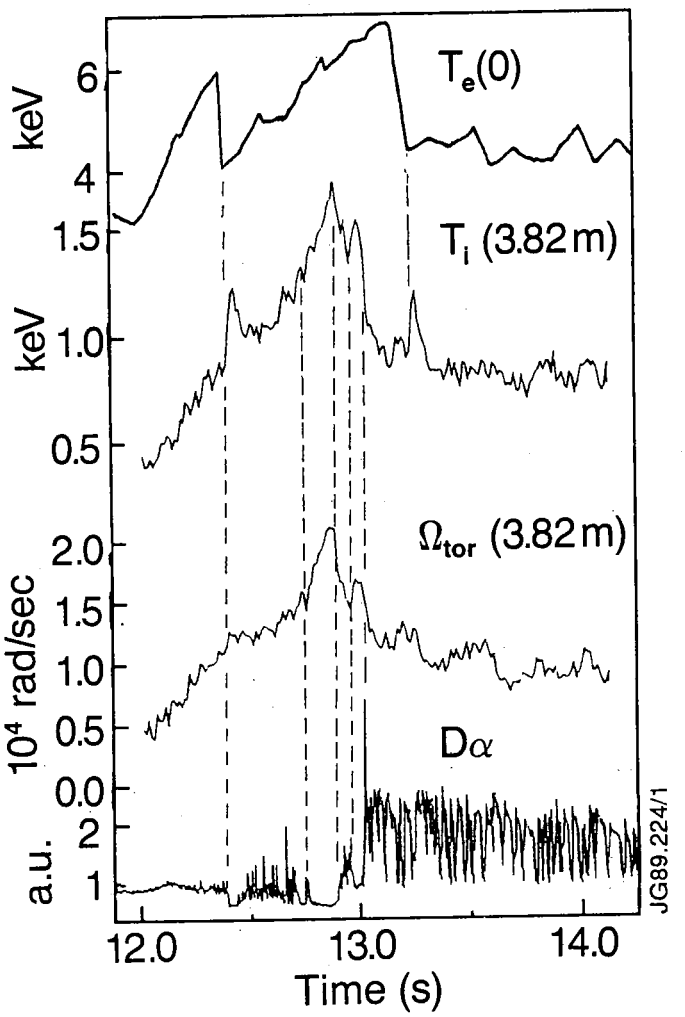

Fig.7 Magnetic limiter discharge with a brief 'ELMy' H-mode. CXS measurement at R=3.82 m of T_i and angular velocity Ω_{tor} with 12 ms resolution. B_T=2.6 T, I_P=5 MA, P_{NBI}=15 MW.

existence of transport mechanisms that are not shared by energy and momentum.

A large set of observations points to the role of MHD modes in momentum transport [29,35]. Fig. 8 shows ion temperature and angular velocity profiles in a plasma with a strong n=1, m=2 mode. Although the ion temperature profiles are fairly peaked, the corresponding angular velocity profiles are flat over the accessible range. In this case the mode was locked (zero frequency) for 0.4 s at the beginning of NBI, then spun up to a maximum angular frequency of $2.5 \cdot 10^4$ rad/sec and finally locked again 0.8 s before the end of NBI. During

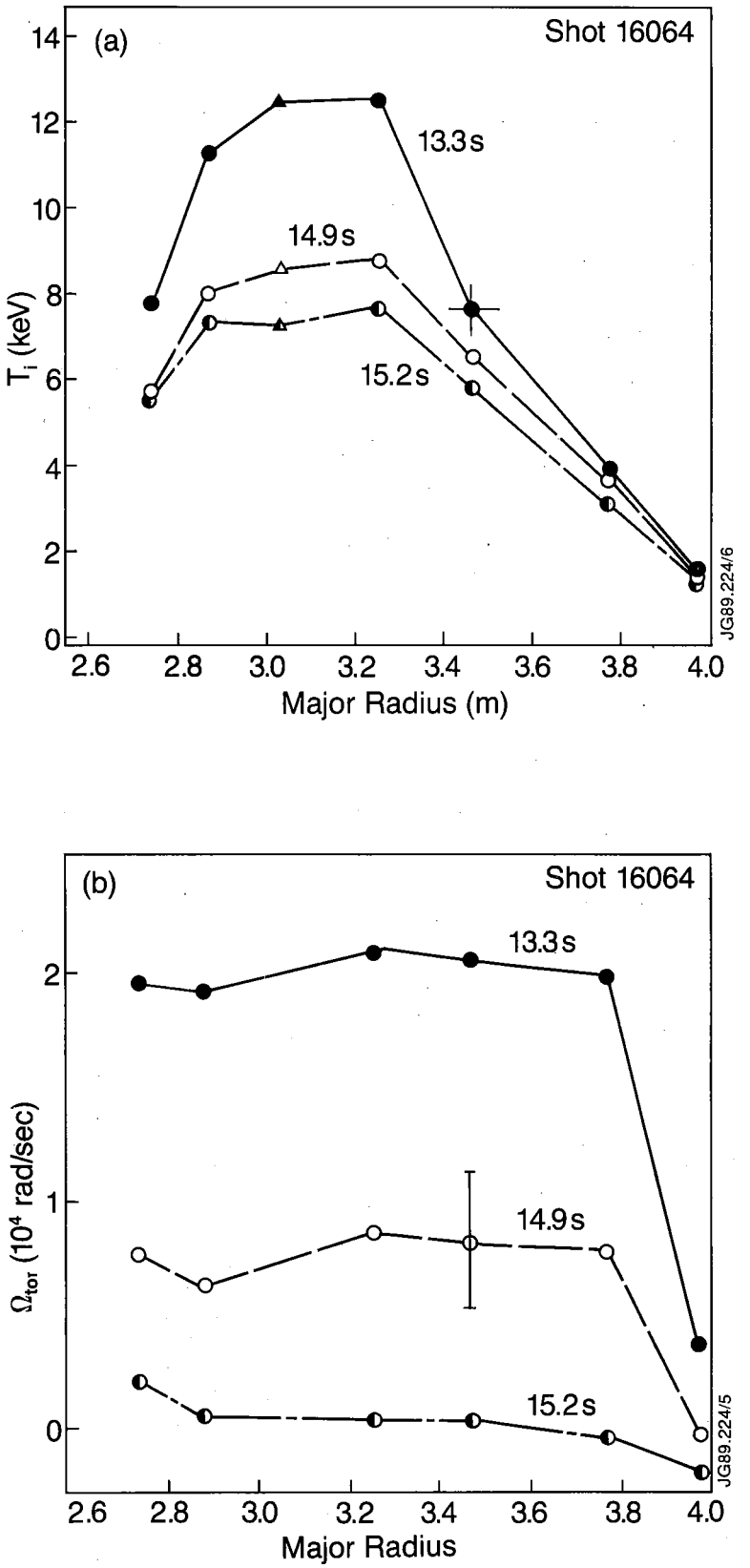

Fig.8 Discharge with strong n=1 MHD activity and locked mode. a) Ion temperature profiles. b) Angular velocity profiles. The mode is rotating at t=13.3 and 14.9 s, it is locked at t=15.2 s.

all three phases the mode angular frequency and the toroidal rotation frequency from charge exchange spectroscopy and from X-ray spectroscopy of Ni XXVII [37] agreed within the errors of the measurements. Flattening and depression of the angular frequency profile, sometimes followed by locking, has been observed in all cases of strong MHD activity for n = 1 and 2 in both limited and diverted discharges. These results show that bulk momentum confinement times can have values from zero up to values of the order of the energy confinement time, depending on MHD activity.

The ions appear to couple to the modes, which in turn are coupled to modes at other rational surfaces in the plasma. Snipes et al [35] have suggested that through a combination of nonlinear coupling (coupling of n-harmonics at the same rational surface) and toroidal or plasma shape induced coupling (coupling of modes at different rational surfaces with equal n, and different m) a dense set of rational surfaces (or magnetic islands thereon) throughout the plasma cross section can be forced to rotate at the same velocity. The modes can interact electromagnetically with the walls by inducing eddy currents which slow down the rotation and with static stray fields which appear to be responsible for their locking [36]. Hence (in addition to viscous diffusion) the toroidal momentum can be lost via a non diffusive transport channel, which it clearly cannot share with the thermal energy.

The existence of a non diffusive transport channel for momentum is corroborated by the absence near the edge of a pulse of toroidal rotation where an ion heat pulse is seen after a sawtooth crash. Unfortunately the existence of central rotation sawteeth is not known for the discharges investigated, such sawteeth have however been observed using X-ray spectroscopy on other JET discharges [37]. We suggest that the transport of toroidal momentum at the crash is also non diffusive, as discussed above, and may be mediated by the n=1, m=1 modes at the q=1 surface, the growth and decay of which is intimately related to sawtooth activity (pre- and postcursor oscillations).

The similarity of electron and ion heat pulses suggests $\chi_i \approx \chi_e$ in the outer region of the discharge, but it is acknowledged that the two cannot easily be separated since the electron - ion equipartition time is only about 20 ms in these conditions. Power balance measurements in these conditions indicate $\chi_e \leq \chi_i \leq 2\chi_e$ [28]. Ion thermal diffusivities have also been obtained indirectly from neutron emission measurements of the ion 'cold front'

propagation following the injection of a small pellet, yielding $\chi_e/3 \leq \chi_i \leq \chi_e$ for R $\cong$ 3.5 m [38].

The often insufficient time resolution of ion temperature diagnostics may convey the (wrong) impression of relatively static ion temperatures. The central ion temperature behaviour from CXS with a resolution of 15 ms, shown in fig. 9 for a hot ion plasma with 10 MW of neutral beam heating demonstrates, not surprisingly, that these discharges are dominated by ion dynamics. Notice the large difference in relative crash amplitude and the expected large difference in heating rates of ions and electrons apparent from the difference in the slopes (dT/dt) early in the sawtooth rise phase. After 50 to 100 ms of strong heating, the ion temperature increase is abrubtly reduced or halted. This event is not observed on the electron temperature.

The ion temperature profile established in this discharge had the peakedness characteristic of hot ion mode NBI-heated plasmas. This suggests that an ion temperature gradient driven instability may be responsible for the loss of ion energy confinement after the brief reheat phase. Since the ion temperature (and to a lesser extend the more moderately peaked density profile) recovers from a flattened profile, the onset of the instability and loss of core confinement may occur when the gradient parameter $\eta_i = d \ln T_i/d \ln n_i$ exceeds a critical value. The present multichannel CXS diagnostic cannot resolve this sequence of events. It provides a sawtooth cycle averaged measurement and thus with $L_{Ti} \leq 0.4$ m near r/a = 0.2 and $L_{ne} \cong$ 0.8 m (from the LIDAR density profile, at t=12.5 s) a lower limit for the above gradient parameter of $\eta_i \geq 2.0$. This is above the threshold predicted by η_i-mode theories. A recent kinetic model including the effect of curvature, e.g., predicts marginal stability for $\eta_i = \eta_{ic} \cong 1 + 2.5(L_n/R - 0.2) \cong 1.1$ for this discharge [39]. Since the ion temperature behaviour seems to suggest saturation near marginal stability at $\eta_{ic} \geq 2$, higher values of η_{ic} would be needed for consistency with theory.

The reheat phase after a sawtooth collapse bears similarities with the reheat phase after the injection of a pellet. In both cases the ion temperatures recover from initially flattened profiles. Pellet injection has been found to lead to substantial enhancements in confinement time, when a peaked density profile was created. It has been suggested that the low values of η_i during the reheat phase are responsible for the improvement [40]. In the pellet case the time resolution of the CXS profile measurements was sufficient to provide η_i because the reheat phase lasted for about 0.6 seconds, due to

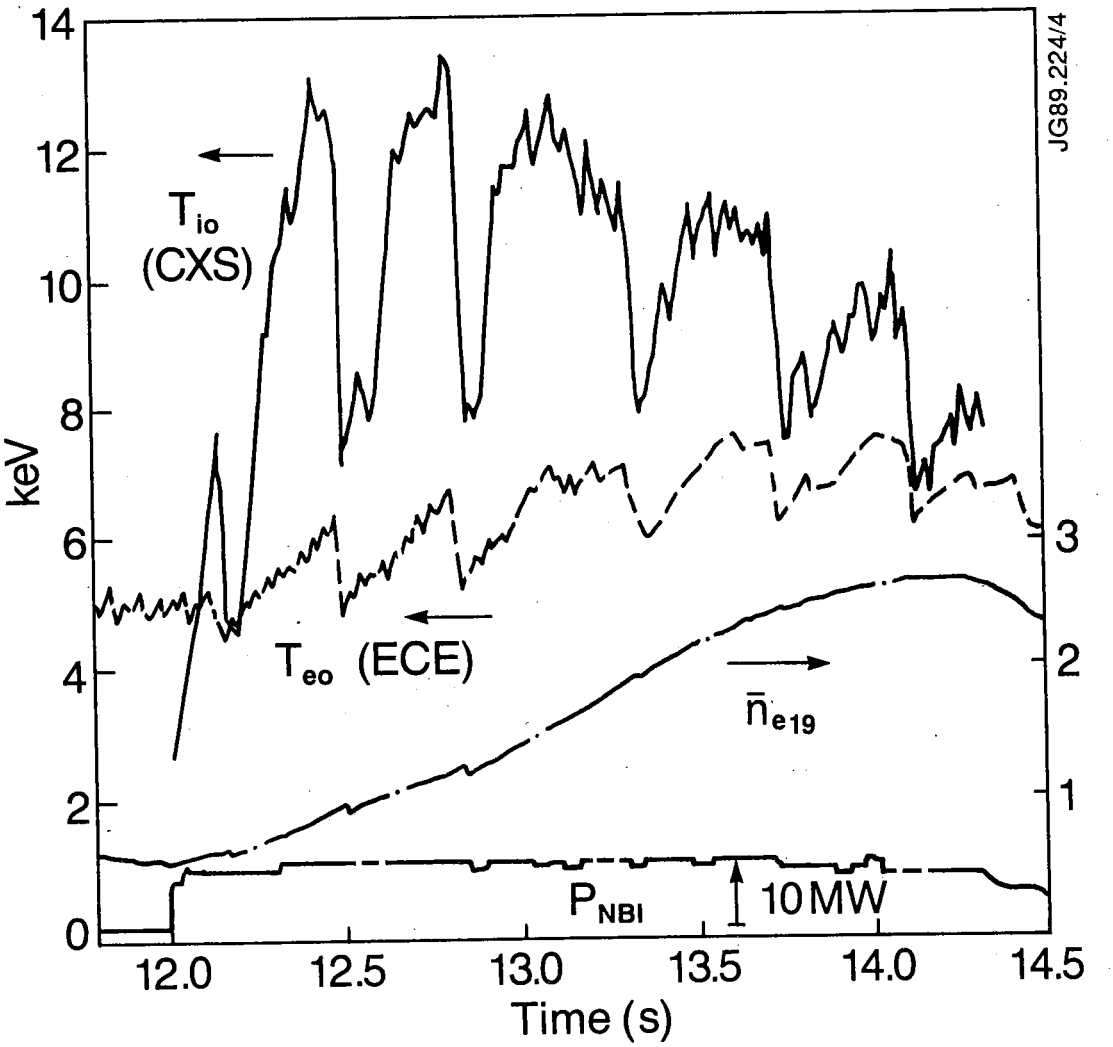

Fig.9 Central ion temperature sawteeth in a hot ion mode plasma.

the high initial density ($n_e(0) \cong 9\times10^{19}m^{-3}$), the low initial temperatures ($T_i \cong T_e \cong 600$ eV), and because both ions and electrons were heated to temperatures above 10 keV. The cases discussed are very different in collisionality. Since collisionality appears not to be a critical parameter in η_i-instability theories, they may explain the observed behavior in both of these cases, provided a reason for the higher threshold is found.

These observations stress the need for ion temperature profile measurements with high time resolution. Such measurements could provide experimental estimates of the ratio of heating rates to ions and electrons, allow to disciminate between different ion energy confinement regimes and fully appreciate the role of sawteeth.

6. CONCLUSIONS

Active charge exchange spectroscopy has proven extremely valuable in determining ion temperatures and toroidal velocities in most JET plasmas. A large variety of profiles has been observed depending on plasma conditions and heating. Our measurements with high time resolution at a single position correlate with transient events in the plasma, such as sawteeth, ELM's and transitions from the L to the H mode and vice versa. They point out important differences between ion energy, toroidal momentum and particle transport, which are often assumed to be closely linked. They urge for a further improvement of the time resolution and its extension to the measurement of the whole profile. The planned implementation of two dimensional CCD arrays is expected to bring the time resolution for profile measurements into the 10 ms range.

Acknowledgements: *We would like to acknowledge the continuous support of Dr W.Engelhardt, and Dr M. Keilhacker for the development of this diagnostic. We greatly appreciated discussions with Dr. P.R. Thomas, Dr N.J. Peacock, J.A. Snipes, J.G. Cordey and other colleagues of the JET team, who also made available their experimental data and calculations of the magnetic geometry, and the support of our technical staff. Special thanks are extended to the NBI team for tailoring NB heating pulses to maximise the use of the beams firing into our viewing lines. Three of us (A.B., L.D.H. and H.W.) would like to acknowledge support, while working at JET, respectively from the Natural Sciences and Engineering Research Council of Canada and The Swiss National Foundation for Scientific Research.*

References

[1] Isler R.C., Murray L.E., Kasai S., Dunlap J.L., Bates S.C., Edmonds P.H., Lazarus E.A., Ma C.H., Murakami M.(1981) Phys. Rev. A **24**, 2701.

[3] Groebner R.J., Brooks F.H., Burrell KH, Rother L.(1983), Appl. Phys. Lett **43**, 920

[2] Isler R.C., Murray L.E.(1983), Appl. Phys. Lett. **25**, 355.

[4] Fonck R.J., Darrow D.S., Jaehnig K.P. (1984) Phys. Rev. A **29**, 3288.

[5] Hawkes N.C., Peacock N.J.(1985), Nucl. Fusion **25**, 971.

[6] Serayadan R.P., Burrell K.H., Brooks N.H., Groebner R.J., Kahn C. (1985) Rev. Sci. Instrum. **57** (2), 155.

[7] Carolan P.G., Duval B.P., Field A.R., Fielding S.J., et al (1987), Phys.Rev.A **35**, 3454.

[8] Burrell K.H., Groebner R.J., John H.St., Seraydarian R.P.(1988), Nuclear Fusion **28**, 3.

[9] Corti S., Boileau A., Bracco G., et al. (1988), 15th Eur.Conf.Contr.Fusion Plasma Phys.,Dubrovnik, ECA **12B**, part I, 127.

[10] Hawkes N.C., von Hellermann M., Boileau A., Horton A., Kaellne E., Peacock N.J., Ramette J., Stork D. (1988), 15th Eur.Conf.Contr.Fusion Plasma Phys.,Dubrovnik, ECA **12B**, part III, 1061.

[11] Von Hellermann M.G., Boileau A., Horton L.D., Summers H.P., Peacock N.J. (1986), Varenna Course and Workshop, CEC, EUR 10797 EN, I, 313.

[12] Von Hellermann M.G., Boileau A., Horton L.D., W. Mandl, Summers H.P., Weisen H. (1989), 16th Eur.Conf.Contr.Fusion Plasma Phys., Venice, ECA **13B**, part I, 107.

[13] Boileau A., von Hellermann M., Horton L.D., Spence J., Summers H.P. (1989) Plasma Phys. Contr. Fusion, **31**, 779.

[14] Boileau A., von Hellermann M., Horton L.D., Summers H.P. Morgan P.D. (1989) *'Low Z impurity behaviour in JET from charge exchange spectroscopy measurements'* Nuclear Fusion, to be published.

[15] Jarvis O.N., Adams J.M., Balet B et al.(1990), *'Determination of deuterium concentrations in JET plasmas'* submitted to Nuclear Fusion.

[16] Von Hellermann M., Summers H., Boileau A. (1988), 15th Eur. Conf. Contr. Fusion Plasma Phys.,Dubrovnik, ECA **12B**, Part III, 1199.

[17] Boileau A., von Hellermann M., Mandl W., Summers H.P. Weisen H., Zinoviev A. (1989) J. Phys. B. **22**, L 145.

[18] The JET Team (1986, presented by Duesing G.), Plasma Phys. Contr. Fusion **28**, 1429.

[19] Boileau A., Von Hellermann M., Horton L.D., Spence J., Summers H.P.(1987) *'The deduction of low-Z ion temperature and densities in the JET tokamak using charge exchange recombination spectroscopy'* JET report JET-P(87)44.

[20] Boileau A., Thèse de doctorat, Université du Québec, INRS-ENERGIE, May 1988.

[21] Core W.G.F. and Cowern C. (1984) *'Influence of neutral injection on the velocity distribution of excited atoms in a plasma'* submitted 1989 to Nuclear Fusion (Letter), also report JET-DN-T(84)42.

[22] Howell R.B., Fonck R.J., Knize R.J., Jaehnig K.P. (1988), Rev. Sci. Instrum. **59** (8), 1521

[23] Ryufuku H.(1982) *'partial cross sections for charge transfer in collisions of multicharged ions with atomic hydrogen'* Japan Atomic Energy Research Institute Report JAERI-M-82-031

[24] Ryufuku H.(1982) Phys. Rev. **A25**, 720.

[25] Fritsch W. (1984), Phys. Rev. **A30**, 3324.

[26] Fritsch W. (1989), Journal de physique, **50**, jan. 1989, C1-87.

[27] De Heer F. and coworkers (1989), FOM Instituut voor Atoom- en Molecuulfysica, Amsterdam, personal communication

[28] The JET Team (1989, presented by Watkins M.L.), 16th Eur. Conf. Contr. Fusion Plasma Phys., Venice.

[29] Snipes J.A., Weisen H., de Esch H.P.L., Galvao R., Hender T.C., Lazzaro Stork D., Von Hellermann M., Zasche D. (1989), 16th Eur. Conf. Contr. Fusion Plasma Phys., Venice, ECA **13B** Vol 2, 513.

[30] The JET Team (1988, presented by Bickerton R.J.), 12th IAEA, Nice.

[31] Tanga A., Behringer K., Costley A. et al (1987) Nuclear Fusion **27**, 1877.

[32] Groebner R.J., Gohil P., Burrell K.H., Osborne T.H., Seraydarian R.P., John H. St.(1989), 16th Eur.Conf.Cont.Fusion.Plasma Phys., Venice, ECA**13B**, I, 245

[33] Hubbard A., Bartlett D., Cripwell P. et al., (1988), 15th Eur. Conf. Plasma Phys. Contr. Fusion, Dubrovnik, ECA Vol. **12B**, part II, 651.

[34] Mattor M., Diamond P.H. (1988), Phys. Fluids **31** (5), 1180.

[35] Snipes J.A., Campbell D.J., Hender T.C., von Hellermann M., Weisen H. (1989) *'Plasma stored energy and momentum losses during large MHD activity in JET'* submitted to Nuclear Fusion.

[36] Snipes J.A., Campbell D.J., Haynes P.S., Hender T.C., Hugon M., et al., (1988) Nuclear Fusion **28**, 1085.

[37] Bartiromo R., Bombarda F., Gianella R., Mantovani S., Panaccione L., Pizzicaroli G.(1989), Rev.Sci.Instrum. **60** (2), 237.

[38] Cheetham A.D., Gondhalekar A., de Haas J.C.M., Jarvis O.N. et al., (1988) 12th IAEA, Nice.

[39] Romanelli F. (1989), Phys. Fluids **B1** (5), 1018.

[40] The JET Team (1988, presented by G.L. Schmidt) 12th IAEA, Nice, Oct. 1988